Calcium Isotopic Compositions of Normal Mid-Ocean Ridge Basalts From the Southern Juan de Fuca Ridge

Hongli Zhu[1], Fang Liu[1,2] (iD), Xin Li[1], Guiqin Wang[1] (iD), Zhaofeng Zhang[1] (iD), and Weidong Sun[3,4,5]

[1]State Key Laboratory of Isotope Geochemistry, Guangzhou Institute of Geochemistry, Chinese Academy of Sciences, Guangzhou, China, [2]University of Chinese Academy of Sciences, Beijing, China, [3]Center of Deep Sea Research, Institute of Oceanography, Chinese Academy of Sciences, Qingdao, China, [4]Laboratory for Marine Mineral Resources, Qingdao National Laboratory for Marine Science and Technology, Qingdao, China, [5]CAS Center for Excellence in Tibetan Plateau Earth Sciences, Chinese Academy of Sciences, Beijing, China

Abstract Mantle peridotites show that Ca is isotopically heterogeneous in Earth's mantle, but the mechanism for such heterogeneity remains obscure. To investigate the effect of partial melting on Ca isotopic fractionation and the mechanism for Ca isotopic heterogeneity in the mantle, we report high-precision Ca isotopic compositions of the normal Mid-Ocean Ridge Basalts (N-MORB) from the southern Juan de Fuca Ridge. $\delta^{44/40}$Ca of these N-MORB samples display a small variation ranging from 0.75 ± 0.05 to 0.86 ± 0.03‰ (relative to NIST SRM 915a, a standard reference material produced by the National Institute of Standards and Technology), which are slightly lower than the estimated Upper Mantle value of 1.05 ± 0.04‰ and the Bulk Silicate Earth (BSE) value of 0.94 ± 0.05‰. This phenomenon cannot be explained by fractional crystallization, because olivine and orthopyroxene fractional crystallization has limited influence on $\delta^{44/40}$Ca of N-MORB due to their low CaO contents, while plagioclase fractional crystallization cannot lead to light Ca isotopic compositions of the residue magma. Instead, the lower $\delta^{44/40}$Ca of N-MORB samples compared to their mantle source is most likely caused by partial melting. The offset in $\delta^{44/40}$Ca between N-MORB and BSE indicates that at least 0.1–0.2‰ fractionation would occur during partial melting and light Ca isotopes are preferred to be enriched in magma melt, which is in accordance with the fact that $\delta^{44/40}$Ca of melt-depleted peridotites are higher than fertile peridotites in literature. Therefore, partial melting is an important process that can decrease $\delta^{44/40}$Ca in basalts and induce Ca isotopic heterogeneity in Earth's mantle.

1. Introduction

Calcium (Ca), the fifth most abundant element in the Earth, has six stable isotopes (^{40}Ca, ^{42}Ca, ^{43}Ca, ^{44}Ca, ^{46}Ca, and ^{48}Ca) with the largest relative mass differences of stable isotopes ($\Delta m/m$ = 20‰) except H and He (DePaolo, 2004; Fantle & Tipper, 2014). The up to ~6‰ variation of Ca isotopic compositions (defined as $\delta^{44/40}$Ca = [(^{44}Ca/^{40}Ca)$_{sample}$/(^{44}Ca/^{40}Ca)$_{NIST-SRM-915a}$ − 1] × 1000) (DePaolo, 2004; Fantle & Tipper, 2014; Heuser & Eisenhauer, 2010) makes Ca an effective geochemical tracer, such as exploring biochemical processes (Chen et al., 2016; Holmden & Bélanger, 2010; Skulan & DePaolo, 1999), investigating the origin of rocky planets and meteorites (Huang & Jacobsen, 2017; Simon & DePaolo, 2010; Simon et al., 2009; Valdes et al., 2014) and mantle Ca isotopic heterogeneity (Kang et al., 2016; Zhao et al., 2017).

With an assumption that Ca isotopic fractionation during partial melting is limited, Huang et al. (2011) used Ca isotopes to trace recycled marine carbonates into the Hawaiian plume based on the differences in $\delta^{44/40}$Ca and CaO content between the mantle and marine carbonates (Fantle & DePaolo, 2005; Farkaš, Böhm, et al., 2007,Farkaš, Buhl, et al., 2007; Griffith et al., 2008). However, the variation of $\delta^{44/40}$Ca in mantle xenoliths and the differences in $\delta^{44/40}$Ca between coexisting pyroxene pairs seemingly point to Ca isotopic fractionation during partial melting (Amini et al., 2009; Feng et al., 2014; Huang et al., 2010; Kang et al., 2016, 2017). For example, Kang et al. (2017) found that $\delta^{44/40}$Ca of melt-depleted peridotites was ~0.1‰ higher than fertile peridotites and attributed this phenomenon to partial melting. Accordingly, light Ca isotopes are likely to be enriched in magma melt (Kang et al., 2016, 2017). To verify whether Ca isotopes could be used as a tracer for recycled marine carbonates in the mantle, it is essential to understand the potential extent of Ca isotopic fractionation that might occur during partial melting.

Mid-ocean Ridge Basalts (MORB) are directly derived from the Upper Mantle without significant crustal contamination. Moreover, the mantle source of MORB samples far away from hot spot is usually less
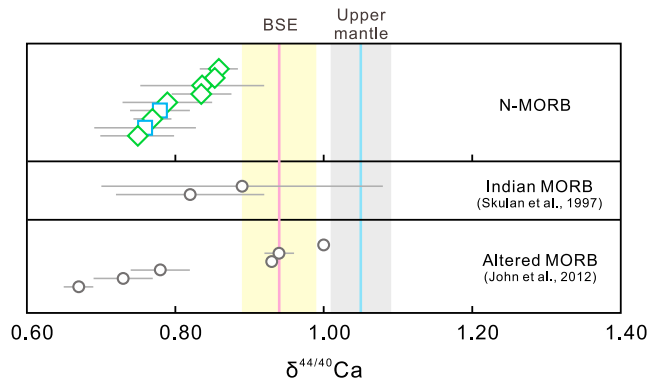
Figure 1. Calcium isotopic compositions of N-MORB samples (green diamonds and blue squares) from the southern Juan de Fuca Ridge (data are reported in Table 1). $\delta^{44/40}$Ca of Indian MORB samples and altered MORB samples in the northwestern Pacific Ocean are reported by Skulan et al. (1997) and John et al. (2012), respectively. The left vertical solid line and bar represent the estimated $\delta^{44/40}$Ca of BSE (0.94 ± 0.05‰) based on measured $\delta^{44/40}$Ca of fertile spinel and garnet peridotites (Kang et al., 2017). The right vertical solid line and bar represent $\delta^{44/40}$Ca of the estimated Upper Mantle (1.05 ± 0.04‰) based on measured $\delta^{44/40}$Ca of pyroxene pairs and mineral assemblage of the Upper Mantle (Huang et al., 2010).

contaminated by enriched components (e.g., recycled marine sediments) than that of Ocean Island Basalts (OIB). Therefore, these normal MORB samples (N-MORB) would provide us a good opportunity to study the behavior of Ca isotopes during partial melting. Nevertheless, to date, few Ca isotope data for fresh MORB samples have been reported, except for two Indian MORB samples and several altered MORB samples from the northwestern Pacific Ocean (Figure 1) (John et al., 2012; Skulan et al., 1997). However, because of the possible influence of recycled marine sediments in the Indian MORB mantle source (Chauvel & Blichert-Toft, 2001; Rehkämper & Hofmann, 1997) or seawater alteration (John et al., 2012), the difference in $\delta^{44/40}$Ca between these reported MORB samples and the Upper Mantle cannot effectively reflect Ca isotopic fractionation during partial melting. Here we report high-precision Ca isotopic compositions of a suite of fresh N-MORB samples from the southern Juan de Fuca Ridge in the east Pacific Ocean. In addition to providing the data set for Ca stable isotopes in fresh MORB samples, our study provides good constraints on the role of partial melting in Ca isotopic fractionation.

2. Samples

N-MORB samples are sampled from the Cleft Segment and the Axial Seamount of the Juan de Fuca Ridge with an intermediate spreading rate. The Cleft Segment, the southernmost portion of this ridge, is relatively unaffected by either "hot spot" melting or enriched mantle sources (Smith & Perfit, 1994). Samples from the Cleft Segment are moderately evolved N-MORB and include very young samples from "Megaplume site" at North Cleft (Embley et al., 1991; Sun et al., 2003). Although the Axial Seamount, which lies in the north of the Cleft Segment, appears to have been influenced by excess magmatism produced by the Cobb melting nearby (Embley et al., 1990; Smith & Perfit, 1994), minor effects on the geochemistry of lavas from this seamount have been observed (Rhodes et al., 1990; Sun et al., 2003). Our results also exclude the possible geochemical influence caused by the Cobb hot spot, because samples from the Axial Seamount have similar trace elements and Sr, Nd, isotope characteristics to the Cleft MORB.

These N-MORB glasses were recovered using the submersible *Alvin*. All of these N-MORB samples are fresh glasses with less than 2% phenocrysts or vesicles. Previous studies found that the phenocryst or microphenocryst phase in MORB samples were olivine (Ol) and plagioclase (Pl) and few pyroxene (Embley et al., 1991; Perfit et al., 1983; Smith & Perfit, 1994). Analyzed glasses were carefully handpicked under a binocular microscope to avoid visible phenocrysts and any alteration in appearance.

3. Analytical Methods

Major and trace elements of N-MORB samples were analyzed by Sun et al. (2003) using a JEOL6400 electron microscope and laser ablation inductively coupled plasma mass spectrometry (LA-ICP-MS) system, respectively. Samples selected from previously prepared glass separates (Sun et al., 2003) were used for Sr, Nd, and Ca isotope analysis. The analytical details of Sr and Nd isotopes are described in supporting information (Text S1). Calcium isotopes were performed at the State Key Laboratory of Isotope Geochemistry, Guangzhou Institute of Geochemistry (GIG), Chinese Academy of Sciences (CAS). Detailed procedures for Ca isotopes have been published in previous studies (Liu, Li, et al., 2017; Zhang et al., 2013; Zhu et al., 2016). Only a brief description is provided below.

N-MORB glasses were crushed and washed ultrasonically in ~1 N HCl and then MQ water for 30 min, respectively. Fresh glasses were handpicked under a binocular microscope. Then they were grounded into 200 mesh powder in an agate mortar. Approximately 80 mg powders were dissolved using a mixture of concentrated HF and HNO_3 with volume ratio of 3:1 in 7 mL Savillex beakers. They were heated on a hotplate at 120°C for at least 5 days. The samples were dried down at 100°C and then were treated with 6 N HCl repeatedly to ensure complete digestion. An aliquot of sample solution that contained ~50 μg Ca was mixed with a certain amount of ^{42}Ca-^{43}Ca double-spike solution. Then this solution was dried down and redissolved

Table 1
Calcium, Sr, and Nd Isotopic Compositions of Studied N-MORB Samples and Standards

	$\delta^{44/40}$Ca						Mean	n[a]	2SD[b]	2SE[c]	^{87}Sr/^{86}Sr[d]	^{143}Nd/^{144}Nd[d]
	1[e]	2	3	4	5	6						
							Juan de Fuca Ridge					
Cleft Segment												
2257-1	0.85	0.86	0.84				0.85	3	0.02	0.01	0.702432	
2257-3	0.84	0.88	0.86				0.86	3	0.04	0.03	0.702422	0.513212
2262-8	0.77	0.79	0.75				0.77	3	0.04	0.02	0.702547	0.513163
2263-6	0.91	0.82	0.77				0.84	3	0.15	0.08	0.702558	0.513157
2269-2	0.71	0.76	0.67	0.72	0.81	0.83	0.75	6	0.12	0.05	0.702544	0.513169
2078-4	0.85	0.81	0.81	0.97			0.86	4	0.15	0.08	0.702528	0.513170
2078-4-R[f]	0.88	0.83	0.79	0.79	0.78		0.81	5	0.08	0.04	0.702529	0.513170
2093-1A	0.83	0.83	0.69	0.80			0.79	4	0.13	0.06	0.702564	0.513144
Axial segment												
XL1739-2A	0.81	0.85	0.71	0.71	0.72		0.76	5	0.12	0.06	0.702583	0.513153
XL1723-1A	0.75	0.75	0.74	0.84	0.81		0.78	5	0.09	0.04	0.702570	0.513154
							Standards					
NIST SRM 915a							0.01	233	0.11	0.01		
IAPSO seawater							1.83	85	0.11	0.01		
BIR-1							0.84	9	0.09	0.03		
BHVO-2							0.80	16	0.12	0.03		
BCR-2							0.82	12	0.07	0.02	0.705007	0.512634
NBS-987											0.710243	
JNdi-1												0.512115

[a]n: number for replicate analyses of Ca isotopes. [b]2SD: two standard deviation. [c]2SE: two standard deviation of the mean. 2SE = 2SD/sqrt (n). [d]External reproducibilities (2SD, two standard deviation) for ^{87}Sr/^{86}Sr and ^{143}Nd/^{144}Nd are 0.000019 and 0.000012, while in-run errors for ^{87}Sr/^{86}Sr and ^{143}Nd/^{144}Nd are better than 0.000008 and 0.000009, respectively. [e]The numbers (1 to 6) represent repeated analyses of the same solution. [f]R: full-procedure duplicate (repeated dissolution and analysis).

in 50 μL of 1.6 N HCl for column chemistry. Calcium was purified using 1 mL Bio-Rad AG MP-50 (100–200 mesh) resin with 1.6 N HCl (Zhu et al., 2016). To check the recovery, precut and after-cut solutions were collected and measured using inductively coupled plasma atomic emission spectrometry (ICP-AES). Results showed that the recovery for each column separation is greater than 99%. During column chemistry, at least one reference material and one blank were processed with samples to monitor the quality of each batch separation.

About 5 μg purified Ca was loaded as calcium nitrate onto an out-gassed (4.5 A for 30 min) 99.995% Ta filament. Calcium isotopic compositions were determined on a thermal ionization mass spectrometry (Thermo Triton) following the procedures documented in Zhu et al. (2016). Instrumental fractionation was corrected by the ^{42}Ca-^{43}Ca double-spike technique using an offline iterative routine with an exponential law similar to Heuser et al. (2002). Each sample was analyzed at least three times. All Ca data are reported as $\delta^{44/40}$Ca relative to NIST SRM 915a. The uncertainties of both two standard deviation (2SD) and two standard deviation of the mean (2SE) are reported in Table 1.

The long-term whole procedural Ca blanks measured by double-spike technique range from 20 to 70 ng, which are usually less than 0.15% of the amount of Ca loaded onto the column. The long-term (since June of 2013) external reproducibility of $\delta^{44/40}$Ca of NIST SRM 915a is 0.01 ± 0.11‰ (2SD, n = 233), and IAPSO (International Association for the Physical Science of the Ocean) seawater is 1.83 ± 0.11‰ (2SD, n = 85) (Table 1). The mean $\delta^{44/40}$Ca values for standard rocks of BIR-1, BHVO-2, and BCR-2 are 0.84 ± 0.09‰ (2SD, n = 9), 0.80 ± 0.12‰ (2SD, n = 16), and 0.82 ± 0.07‰ (2SD, n = 12), respectively (Table 1). All these results are in consistent with the data reported by previous studies (Amini et al., 2009; Feng et al., 2017; He et al., 2017; Holmden & Bélanger, 2010; Huang et al., 2010; Liu, Li, et al., 2017; Valdes et al., 2014). One sample (2078-4) was replicated by digestion of separate glass, showing great reproducibility in Ca isotopic values (Table 1).

4. Results

Calcium, Sr, and Nd isotopic compositions for N-MORB samples from the southern Juan de Fuca Ridge are reported in Table 1. Major and trace element concentrations adopted from Sun et al. (2003) are listed in Table S1.

N-MORB normalized trace element abundance patterns and chondrite-normalized REE (rare earth element) patterns of our N-MORB samples are shown in Figures S1 and S2 (Sun et al., 2003; Sun & McDonough, 1989). They show flat REE patterns with slight LREE (light rare earth element) depletion in chondrite-normalized (Sun & McDonough, 1989) diagrams (Figure S2) (Sun et al., 2003). There are small variations in $^{87}Sr/^{86}Sr$ and $^{143}Nd/^{144}Nd$ ratios (Table 1), with an average of 0.70253 ± 0.00012 (2SD, n = 9) and 0.51317 ± 0.00004 (2SD, n = 9), respectively, which are similar to that of the depleted MORB mantle (Workman & Hart, 2005). The $\delta^{44/40}Ca$ values of these N-MORB glasses vary from 0.75 ± 0.05 (2SE) to 0.86 ± 0.03‰ (2SE) (Table 1). Compared to the reported Ca isotopic compositions of altered MORB samples from the northwestern Pacific Ocean that ranged from 0.73 ± 0.04 (2SE) to 1.00‰ (John et al., 2012), our studied N-MORB glasses display a smaller range of variation (Figure 1). Notably, these Ca isotope data of N-MORB samples are lower than that of the estimated Bulk Silicate Earth (BSE) (0.94 ± 0.05‰) and the Upper Mantle (1.05 ± 0.04‰) (Figure 1).

5. Discussion

5.1. Calcium Isotopic Compositions of the N-MORB Mantle Source

To explore the effects of partial melting on Ca isotopic fractionation from the aspect of N-MORB samples, a comparison of $\delta^{44/40}Ca$ between N-MORB samples and their mantle source is necessary. Therefore, $\delta^{44/40}Ca$ of their mantle source should be evaluated and constrained first. To date, the Ca isotopic composition of the Upper Mantle is poorly constrained due to the limited Ca isotope data for mantle peridotites. $\delta^{44/40}Ca$ in oceanic basalts with large variations (>0.7‰) (e.g., Amini et al., 2009; DePaolo, 2004; Simon & DePaolo, 2010; Valdes et al., 2014) cannot exactly mirror the $\delta^{44/40}Ca$ of the Upper Mantle, because of the potential isotopic fractionation during partial melting (Kang et al., 2016, 2017).

Based on $\delta^{44/40}Ca$ of clinopyroxene (Cpx) and orthpyroxene (Opx) in peridotites (Huang et al., 2010) and the Upper Mantle mineral assemblage, that is, 13–18% Cpx and 32–27% Opx (Salters & Stracke, 2004; Workman & Hart, 2005), Huang et al. (2010) estimated $\delta^{44/40}Ca$ of the Upper Mantle with a value of 1.05 ± 0.04‰ (ranging from 1.02 to 1.08‰). Yet this value should by no means be regarded as final since the limited number of samples analyzed (Huang et al., 2010). Recently, according to the average of $\delta^{44/40}Ca$ in 14 fertile peridotites (e.g., garnet, garnet-spinel, and spinel lherzolites) that without significant modification by partial melting or metasomatism, Kang et al. (2017) estimated $\delta^{44/40}Ca$ of the BSE to be 0.94 ± 0.05‰ (2SD).

MORB samples are formed directly by partial melting of the Upper Mantle. Compared to the primitive mantle or BSE, the depleted Upper Mantle (DMM) has been depleted by melt extraction (Workman & Hart, 2005). Because melt extraction might progressively increase $\delta^{44/40}Ca$ of the residue (Amini et al., 2009; Kang et al., 2016, 2017), $\delta^{44/40}Ca$ of the N-MORB mantle source would be consequently higher than the estimated BSE of 0.94 ± 0.05‰ (2SD) (Kang et al., 2017). Thus, our studied N-MORB samples have lighter Ca isotopic compositions than that of their mantle source. There is at least about 0.1–0.2‰ offset between these N-MORB samples and their mantle source.

5.2. Possible Processes to Lower $\delta^{44/40}Ca$ of N-MORB Samples

In general, a variety of geological processes could occur during the formation of N-MORB samples, including seawater alteration for submarine glasses, fractional crystallization during magma ascent, and mantle partial melting, which would possibly deviate Ca isotopic compositions of N-MORB samples from their mantle source. Processes that may cause the $\delta^{44/40}Ca$ differences between N-MORB samples observed in this contribution and their mantle sources are discussed below.

5.2.1. Seawater Alteration

Seawater alteration and serpentinization are important processes, which might modify the Ca isotopic compositions of oceanic crust and peridotite. A previous study found that Ca isotopic compositions are negatively correlated with loss on ignition of serpentinized slab mantle rocks, indicating that $\delta^{44/40}Ca$ of serpentinite decreases with increasing degree of serpentinization (alteration) (John et al., 2012). The large variation of $\delta^{44/40}Ca$ in altered MORB samples from the northwestern Pacific Ocean (0.67–1.0‰) might also be caused by seawater alteration (Figure 1) (John et al., 2012). However, our N-MORB samples are fresh without any seawater alteration, which is supported by several lines of evidence.

First, these N-MORB samples did not show K or Rb positive anomalies (Verma, 1992). Second, $^{87}Sr/^{86}Sr$ of these N-MORB samples displayed a little variation with an average of 0.70253 ± 0.00012 (2SD, n = 9), which are

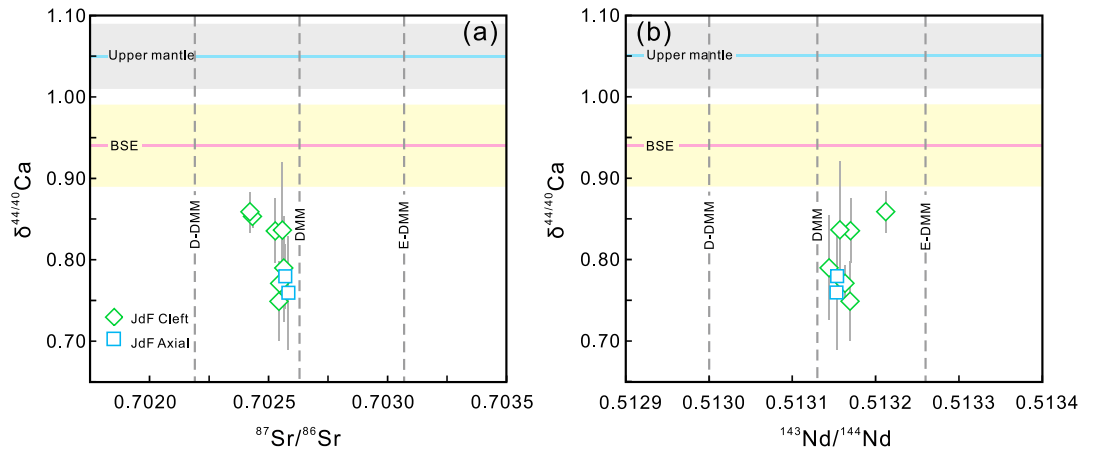**Figure 2.** $\delta^{44/40}$Ca versus ^{87}Sr/^{86}Sr and ^{143}Nd/^{144}Nd of the N-MORB samples. The vertical dashed lines represent ^{87}Sr/^{86}Sr and ^{143}Nd/^{144}Nd of D-DMM, DMM, and E-DMM (Workman & Hart, 2005). The horizontal yellow and gray bars represent $\delta^{44/40}$Ca of the estimated Upper Mantle and BSE (Huang et al., 2010; Kang et al., 2017), respectively. DMM: the depleted MORB mantle; JdF: the Juan de Fuca Ridge.

similar to the depleted MORB mantle (Workman & Hart, 2005) (Figure 2a). If these N-MORB samples experienced apparent seawater alteration, they should tend to be with higher ^{87}Sr/^{86}Sr values than the depleted MORB mantle (Verma, 1992). In addition, previous studies have shown that U/Th and U/Pb ratios in MORB samples would increase with seawater alteration (Verma, 1992). In this study, U/Th and U/Pb ratios show limited variations and are similar to that of N-type MORB reported by Sun and McDonough (1989). Moreover, none of these ratios show covariation with $\delta^{44/40}$Ca (Figure S3). Taken together, seawater alteration cannot account for the low $\delta^{44/40}$Ca signature of our N-MORB samples.

5.2.2. Fractional Crystallization

MORB samples are considered to represent the residue melt that has evolved primarily through fractional crystallization of Ol, Opx, or Pl as a result of cooling at shallow levels (Niu, 1997; Price et al., 1986; Smith & Perfit, 1994). Exploring the effect of fractional crystallization on Ca isotopic compositions is essential to understand whether $\delta^{44/40}$Ca of evolved MORB samples could represent that of their primitive magma.

Previous studies observed that Ol and Opx tend to be enriched in heavier Ca isotopes than Cpx and consequently have higher $\delta^{44/40}$Ca than Cpx (Huang et al., 2010; Kang et al., 2016). This phenomenon is consistent with the theoretical study that heavier isotopes are preferred in stronger bonding environment (Urey, 1947). Because the coordination number of Ca is 6 in Ol and Opx and 8 in Cpx, the Ca-O bonds in Ol and Opx are stronger than Cpx (Huang et al., 2010; Magna et al., 2015). Even so, Ol and Opx fractional crystallization should have little effect on $\delta^{44/40}$Ca of N-MORB samples because of their relatively low CaO contents. This is evidenced by a simple mass balance calculation shown in Figure 3, which displays that Ol and Opx fractional crystallization cannot lead to significant Ca isotopic fractionation. Detailed information of our calculation is given in the supporting information (Text S2). Based on the $\delta^{44/40}$Ca of Ol and dunite standard DTS-1 (Amini et al., 2009; Kang et al., 2016) and CaO content in Ol (Kamenetsky et al., 1998; Sobolev et al., 2007), our calculation predicts that $\delta^{44/40}$Ca of the residue magma would only decrease by 0.01‰ when magma experiences 50% Ol fractionation (Figure 3). Similarly, based on the $\delta^{44/40}$Ca and CaO concentration in Opx (Huang et al., 2010; Kang et al., 2016), $\delta^{44/40}$Ca of the residue magma would only decrease by at most 0.03‰ when magma experiences 50%

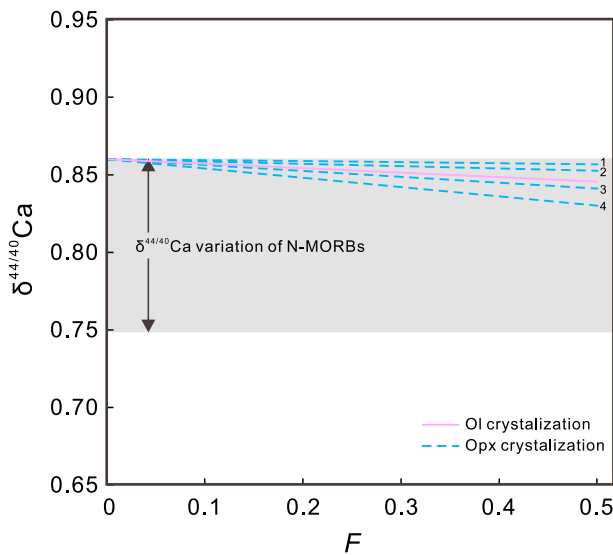**Figure 3.** The estimated impact of Ol and Opx fractional crystallization on $\delta^{44/40}$Ca of N-MORB samples based on mass balance calculation. F means the mass fraction of separated crystal. In this mass balance calculation, $\delta^{44/40}$Ca of primitive magma is supposed to be 0.86‰, which is the highest value of studied N-MORB samples. The solid pink line represents the influence caused by different extents of Ol fractional crystallization with $\delta^{44/40}$Ca = 1.5‰ and CaO = 0.5 wt.%. The dashed blue lines represent the influence caused by different extents of Opx fractional crystallization with different $\delta^{44/40}$Ca and CaO contents, and the numbers (1 to 4) represent different Opx from Huang et al. (2010) and Kang et al. (2016). For example, 1, 2, and 3 refer to the samples of P-10, H-16, and P-9 (Kang et al., 2016), and 4 refers to the Opx from Kibourne Hole (Huang et al., 2010). The gray shaded area represents the $\delta^{44/40}$Ca variation of N-MORB samples.
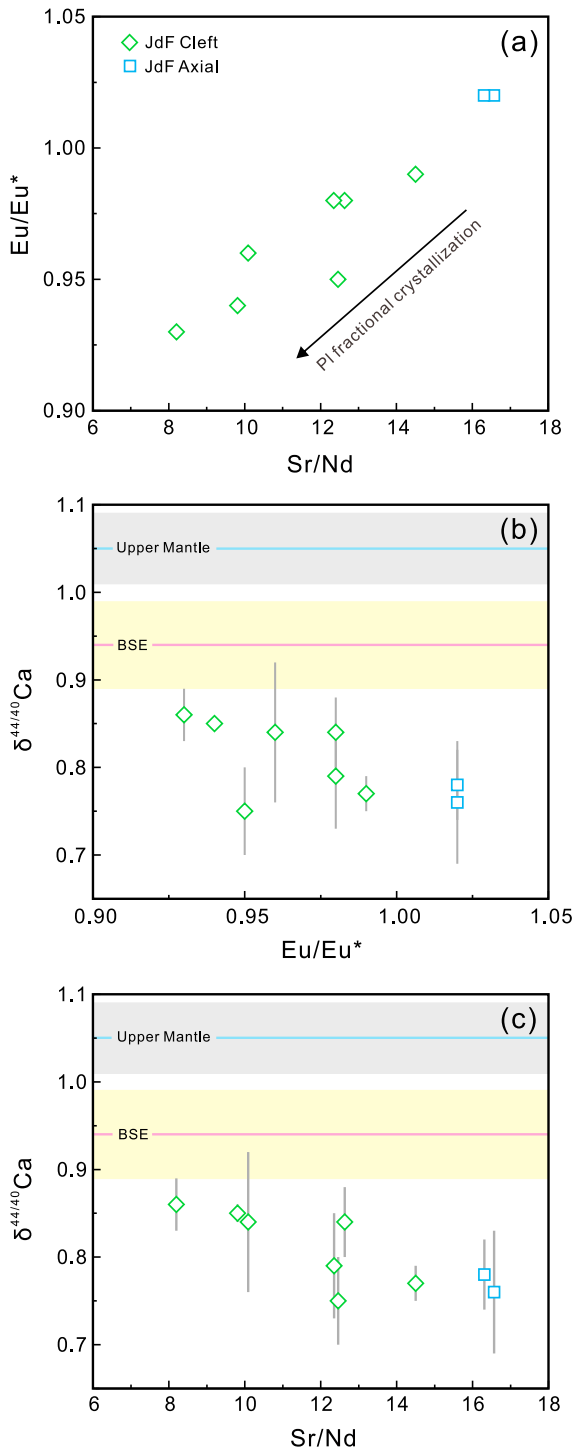
Figure 4. (a) Eu/Eu* versus Sr/Nd, (b) $\delta^{44/40}$Ca versus Eu/Eu*, and (c) $\delta^{44/40}$Ca versus Sr/Nd of N-MORB samples. Panel a shows the positive correlation between Eu/Eu* and Sr/Nd, which indicates the possibility of Pl fractional crystallization. Panels b and c show the correlations between $\delta^{44/40}$Ca and Eu/Eu* and Sr/Nd ratios. The horizontal yellow and gray bars in panels b and c represent $\delta^{44/40}$Ca of the estimated Upper Mantle and BSE (Huang et al., 2010; Kang et al., 2017), respectively. Eu/Eu* = $w(Eu)_N/(w(Sm)_N \times w(Gd)_N)^{1/2}$; N refers to CI chondrite-normalized data that adopts from Sun and McDonough (1989). JdF: the Juan de Fuca Ridge.

Opx fractionation (Figure 3). Compared to the scale of $\delta^{44/40}$Ca variation in N-MORB samples, Ca isotopic fractionation caused by Ol and Opx fractional crystallization is negligible (Figure 3). Thus, these processes are not responsible to the 0.1–0.2‰ offset of $\delta^{44/40}$Ca between these N-MORB samples and their mantle source.

MORB samples usually experienced Pl fractional crystallization (Nauret et al., 2006). Europium anomaly (defined as Eu/Eu*; see caption of Figure 4 for equation) and Sr/Nd ratios can be used to assess Pl fractional crystallization, because Eu and Sr have high partition coefficient in Pl (Nauret et al., 2006). For our N-MORB samples, Eu/Eu* is positively correlated with Sr/Nd (Figure 4a), indicating the possibility of Pl fractional crystallization. It is worth noting that these N-MORB samples show flat REE patterns (Figure S2) without significant Eu anomalies. Only samples from the Cleft Segment have slightly negative Eu anomaly with Eu/Eu* range from 0.93 to 0.99. Besides, these samples also show a small variation in Sr contents (93 to 117 ppm). Thereby, the degree of Pl fractional crystallization should be small. However, in Figures 4b and 4c, $\delta^{44/40}$Ca of N-MORB samples seem to be negatively correlated with Eu/Eu* and Sr/Nd ratios. Even if such negative trends are indeed caused by Pl fractional crystallization, $\delta^{44/40}$Ca of N-MORB samples would increase during this process. Therefore, the lower $\delta^{44/40}$Ca of N-MORB samples (0.75 ± 0.05 to 0.86 ± 0.03‰) compared to their mantle source (~0.94‰) (Figure 2) cannot be explained by Pl fractional crystallization.

Additionally, recent studies did not observe significant fractionation of $\delta^{44/40}$Ca during the evolution of mafic and intermediate magma, such as Pl fractional crystallization (e.g., Amini et al., 2009; Chen et al., 2014; Liu, Li, et al., 2017). Specifically, Chen et al. (2014) found that cogenetic samples from the Canary Islands have similar $\delta^{44/40}$Ca despite of a substantial chemical variability. Similarly, Amini et al. (2009) and Liu, Zhu, et al. (2017) did not observe large Ca isotopic variations in intermediate-mafic reference rocks. These observations exclude the possible effect of fractional crystallization (e.g., Ol, Opx, and Pl) on $\delta^{44/40}$Ca during intermediate-mafic magma evolution.

5.2.3. Partial Melting

Equilibrium isotopic fractionation during partial melting is different in different stable isotope systems. For example, the indistinguishable Mg isotopic compositions among global MORB, OIB, and peridotites suggest insignificant Mg isotopic fractionation during partial melting (Teng et al., 2010), while the ~0.1‰ difference of δ^{56}Fe between MORB and mantle peridotites indicates that Fe isotopic fractionation would occur during partial melting (Dauphas et al., 2009; Weyer & Ionov, 2007). Up to now, the Ca isotopic fractionation during partial melting has not been well constrained. Although previous studies demonstrated that melt extraction may increase $\delta^{44/40}$Ca of the residues by comparing $\delta^{44/40}$Ca between the fertile peridotites and melt-depleted, unmetasomatized peridotites (Kang et al., 2016, 2017), direct evidence from magma melt is still scarce.

Because recycled marine carbonates with lower $\delta^{44/40}$Ca would decrease $\delta^{44/40}$Ca (e.g., Chen et al., 2014; Huang et al., 2011), the large variation of $\delta^{44/40}$Ca in OIB (>0.7‰) and the offset between OIB and the estimated Upper Mantle or BSE cannot be merely attributed to partial melting (Chen et al., 2014; Kang et al., 2017). Compared to OIB samples, our N-MORB samples are far from hot spot; thus, they are less contaminated by hot spot materials (Rhodes et al., 1990; Smith & Perfit, 1994;
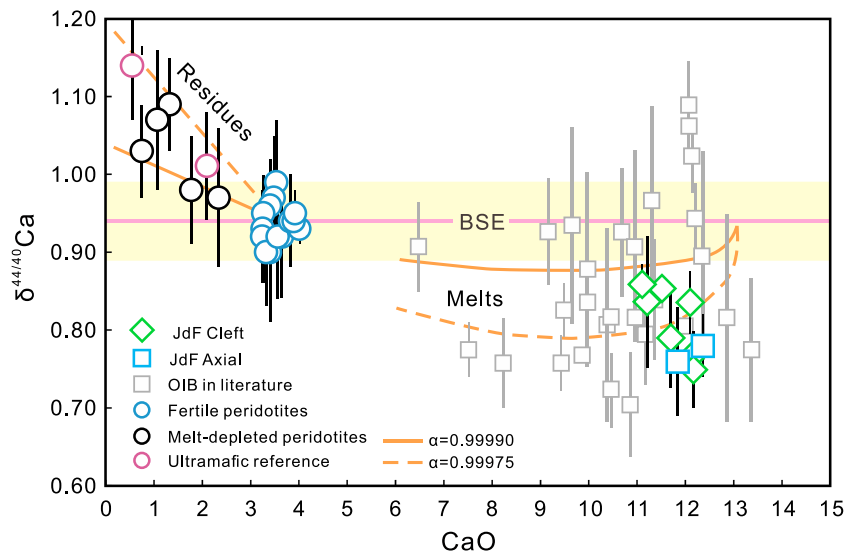
Figure 5. Comparison of N-MORB and OIB with mantle peridotites on a plot of $\delta^{44/40}$Ca versus CaO. The horizontal solid line and bar represent $\delta^{44/40}$Ca of the BSE that based on fertile peridotites (Kang et al., 2017). The solid and dashed yellow lines represent recent modeling results for residues and partial melts of pure batch melting of the BSE with $\alpha_{peridotite-melt}$ ranging from 0.99990 to 0.99975 (Kang et al., 2017). OIB data are from Amini et al. (2009), Huang et al. (2011), Jacobson et al. (2015), and Valdes et al. (2014). Fertile and melt-depleted peridotites data are from Kang et al. (2017). Ultramafic reference data are from Amini et al. (2009).

Sun et al., 2003). Compared to the scale of Sr and Nd isotopic variations in the Upper Mantle (Workman & Hart, 2005), our N-MORB samples display quite small variations in ^{87}Sr/^{86}Sr and ^{143}Nd/^{144}Nd ratios (Figure 2). They show similar Sr and Nd isotopic compositions to that of the depleted MORB mantle (Workman & Hart, 2005), which further excludes the influence of recycled marine carbonates. Consequently, our N-MORB samples are good candidates to explore the behavior of Ca isotopes during partial melting and the potential extent of Ca isotopic fractionation, if any.

5.2.3.1. Low $\delta^{44/40}$Ca Signature in N-MORB Induced by Partial Melting

As discussed in section 5.1, at least 0.1–0.2‰ offset of $\delta^{44/40}$Ca exists between our N-MORB samples and their mantle source (Figure 2). Since no seawater alteration was observed and fractional crystallization of Ol, Opx, and Pl cannot cause such low $\delta^{44/40}$Ca signature of N-MORB samples, we propose that this offset should be attributed to partial melting. If partial melting of the Upper Mantle can cause the low $\delta^{44/40}$Ca signature of melts, the residue peridotites should tend to have heavier Ca isotopic compositions. This is consistent with the observations that $\delta^{44/40}$Ca of mantle peridotites and ultramafic reference samples that experienced melt extraction are higher than the estimated BSE (Amini et al., 2009; Kang et al., 2017). For example, $\delta^{44/40}$Ca of the strongly melt-depleted, unmetasomatized harzburgites with low CaO contents are ~0.1‰ higher than that of the fertile peridotites without significant modification by melting or metasomatism (Figure 5) (Kang et al., 2017). $\delta^{44/40}$Ca of some ultramafic reference materials (e.g., BM90/21-G and PCC-1) are 0.06 to 0.2‰ higher than the estimated BSE (Figure 5) (Amini et al., 2009). That is to say, $\delta^{44/40}$Ca values of peridotites would be influenced by melt extraction and usually increased with melt extraction (Kang et al., 2017). Taken together, during partial melting, light Ca isotopes are preferentially incorporated into magma melt (e.g., MORB samples), while the heavy ones prefer to stay in the residue (e.g., melt-depleted peridotites) (Figure 5). Additionally, $\delta^{44/40}$Ca of our N-MORB samples are consistent with modeling results for partial melts of pure batch melting of the BSE with $\alpha_{peridotite-melt}$ (the fractionation factor between peridotite and melt) ranging from 0.99990 to 0.99975 ($10^3 \ln \alpha_{peridotite-melt} \approx 0.10$–0.25) by Kang et al. (2017) (Figure 5), which further suggest that at least 0.1–0.2‰ Ca isotopic fractionation would occur during partial melting.

The behavior of Ca isotopes during partial melting might be caused by the differences in $\delta^{44/40}$Ca among minerals in the mantle source and melting priority of these minerals (Green, 1973; Huang et al., 2010; Jaques & Green, 1980; Kang et al., 2016, 2017; Zhao et al., 2017). Earlier studies have observed −0.01‰ to 1.11‰ differences in $\delta^{44/40}$Ca between coexisting Cpx and Opx, the two major Ca-bearing minerals in the
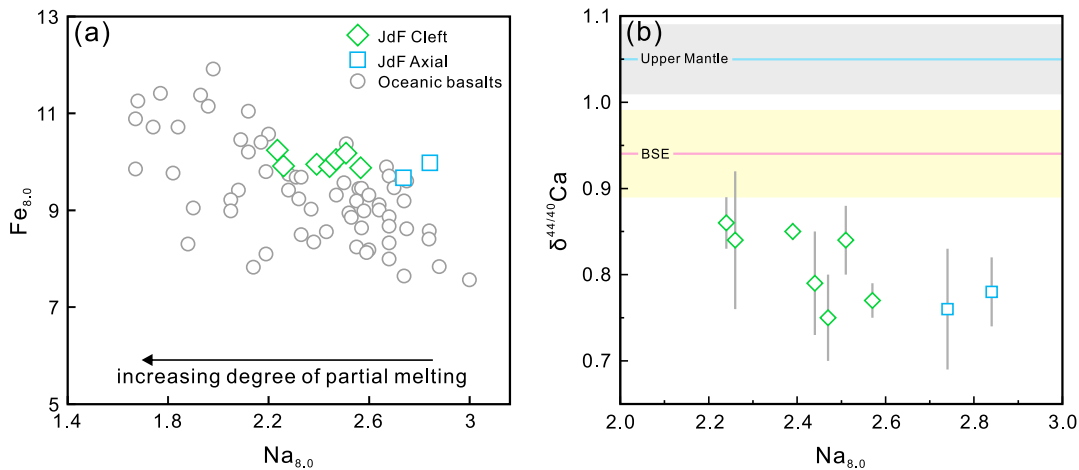
Figure 6. (a) $Fe_{8.0}$ versus $Na_{8.0}$ and (b) $\delta^{44/40}Ca$ versus $Na_{8.0}$ in studied N-MORB samples. $Fe_{8.0}$ and $Na_{8.0}$ are calculated for samples with MgO content between 5.0 and 8.5 wt.% only, using the formulae adopted from Klein and Langmuir (1987): $Na_{8.0} = Na_2O + 0.373 \times (MgO) - 2.98$; $Fe_{8.0} = FeO + 1.664 \times (MgO) - 13.313$. The global oceanic basalts in panel a are adopted from Klein and Langmuir (1987). The horizontal yellow and gray bars in panel b represent $\delta^{44/40}Ca$ of the estimated Upper Mantle and BSE (Huang et al., 2010; Kang et al., 2017), respectively. JdF: the Juan de Fuca Ridge.

Upper Mantle (Huang et al., 2010; Kang et al., 2016; Zhao et al., 2017). In general, Cpx has lighter Ca isotopic compositions than coexisting Opx and Ol (Huang et al., 2010; Kang et al., 2016; Zhao et al., 2017). Melting experiments on the mantle peridotites indicated that Cpx tends to be consumed more rapidly than Opx in the residue during partial melting (Green, 1973; Jaques & Green, 1980), then light Ca isotopes from Cpx would be easily transferred to the melt, while the heavy ones from Opx and Ol are preferred to stay in the residue, which is in great agreement with our data for N-MORB samples and melt-depleted peridotites in literature (Kang et al., 2016, 2017).

5.2.3.2. The Influence of Different Melting Degrees on $\delta^{44/40}Ca$ Variations of N-MORB

To explore the influence of different partial melting degrees on $\delta^{44/40}Ca$ of N-MORB, it is critical to find a proper proxy to quantitatively constrain the degree of partial melting. At small degrees of partial melting, incompatible/compatible trace element ratios (e.g., La/Yb, Nb/Y, and Ba/Y) generally decrease with increasing partial melting degrees. But these ratios will become less sensitive when the degree of partial melting increases. For MORB samples, they usually formed at high degrees of partial melting of the Upper Mantle (e.g., 20%) (Klein & Langmuir, 1987), so incompatible/compatible trace element ratios might not be the sensitive proxy for partial melting degrees of MORB samples. Instead, Na behaves as a moderately incompatible element, showing higher concentrations at smaller extents of melting and decreasing in concentration by dilution as the extent of melting increases (Fujii & Scarfe, 1985; Jaques & Green, 1980). Therefore, the $Na_{8.0}$ content of MORB samples, which means the calculated Na_2O content at MgO = 8 wt.% to remove fractionation effect (see caption of Figure 5 for equation), might be a suitable proxy to constrain the degree of partial melting (Klein & Langmuir, 1987). For our samples, there is an ~0.6 difference in $Na_{8.0}$ ranging from 2.2 to 2.8, indicating an ~3.5% difference in melting degrees (Bezard et al., 2016).

The oceanic basalts display a global negative correlation between $Na_{8.0}$ and $Fe_{8.0}$ (the calculated FeO content at MgO = 8 wt.%; see caption of Figure 5 for equation), which is generally controlled by partial melting (Bezard et al., 2016; Klein & Langmuir, 1987). Our N-MORB samples form a flat to slightly negative correlation between $Na_{8.0}$ and $Fe_{8.0}$ (Figure 6a) but fall on the negative trend defined by the global oceanic basalts (Klein & Langmuir, 1987), which reflects the control of partial melting (Bezard et al., 2016; Klein & Langmuir, 1987). In Figure 6b, $\delta^{44/40}Ca$ is negatively correlated with $Na_{8.0}$ ($R^2 = 0.46$), suggesting that under the partial melting degrees of the MORB mantle source (e.g., 10–20%), $\delta^{44/40}Ca$ of N-MORB samples increase with increasing of partial melting degrees. Assuming that the MORB mantle source experienced 100% melting, $\delta^{44/40}Ca$ of the melts should be identical to their mantle source, which is consistent with the trend we observed in Figure 6b.

As discussed in section 5.2.2, the $\delta^{44/40}Ca$ variation (0.75 ± 0.05 to 0.86 ± 0.03‰) measured in N-MORB samples seems negatively correlated with Eu/Eu* and Sr/Nd ratios (Figures 4b and 4c), which suggests that

Pl fractional crystallization may also play a role in the $\delta^{44/40}$Ca variation of N-MORB samples. However, it should be noticed that these samples only experienced small extent of Pl fractional crystallization, so that this process may have little effect on $\delta^{44/40}$Ca of our studied N-MORB samples. Limited by our number of samples, we cannot quantitatively evaluate the influence induced by Pl fractional crystallization. More detailed works are therefore needed in the future.

6. Conclusions

Calcium isotopic compositions of N-MORB samples from the southern Juan de Fuca Ridge exhibit a small variation that ranged from 0.75 ± 0.05 to 0.86 ± 0.03‰. They are lower than that of their mantle source. Seawater alteration and fractional crystallization of Ol, Opx, and Pl were excluded for causing the low $\delta^{44/40}$Ca signature of N-MORB samples. Instead, the lighter Ca isotopic signature of N-MORB samples compared to their mantle source is most likely induced by partial melting. During partial melting, the lighter Ca isotopes are preferentially incorporated into magma melt, which is in accordance with the fact that $\delta^{44/40}$Ca of peridotites increases with partial melting in literature. Moreover, the difference of $\delta^{44/40}$Ca between N-MORB samples and their mantle source is also in agreement with recent modeling results for partial melts of pure batch melting of the BSE by Kang et al. (2017), further implying that at least 0.1–0.2‰ Ca isotopic fractionation would be caused by partial melting. Therefore, partial melting plays an important role in generating the Ca isotopic heterogeneity in Earth's mantle. This process should also be considered cautiously when using Ca isotopes in mantle-derived basalts to trace recycled marine carbonates in the mantle source, because it can reduce $\delta^{44/40}$Ca in mantle-derived basalts.

References

Amini, M., Eisenhauer, A., Böhm, F., Holmden, C., Kreissig, K., Hauff, F., & Jochum, K. P. (2009). Calcium isotopes ($\delta^{44/40}$Ca) in MPI-DING reference glasses, USGS rock powders and various rocks: Evidence for Ca isotope fractionation in terrestrial silicates. *Geostands and Geoanalytical Research*, *33*(2), 231–247. https://doi.org/10.1111/j.1751-908X.2009.00903.x

Bezard, R., Fischer-Gödde, M., Hamelin, C., Brennecka, G. A., & Kleine, T. (2016). The effects of magmatic processes and crustal recycling on the molybdenum stable isotopic composition of Mid-Ocean Ridge Basalts. *Earth and Planetary Science Letters*, *453*, 171–181. https://doi.org/10.1016/j.epsl.2016.07.056

Chauvel, C., & Blichert-Toft, J. (2001). A hafnium isotope and trace element perspective on melting of the depleted mantle. *Earth and Planetary Science Letters*, *190*(3-4), 137–151. https://doi.org/10.1016/S0012-821X(01)00379-X

Chen, X., Deng, W., Zhu, H., Zhang, Z., Wei, G., & McCulloch, M. T. (2016). Assessment of coral $\delta^{44/40}$Ca as a paleoclimate proxy in the Great Barrier Reef of Australia. *Chemical Geology*, *435*, 71–78. https://doi.org/10.1016/j.chemgeo.2016.04.024

Chen, H., Savage, P. S., Valdes, M., Puchtel, I. S., Day, J. M. D., Moreira, M., et al. (2014). Heterogeneity of calcium isotopes in Earth's mantle, Goldschmidt 2014 Abstracts, 400, California.

Dauphas, N., Craddock, P. R., Asimow, P. D., Bennett, V. C., Nutman, A. P., & Ohnenstetter, D. (2009). Iron isotopes may reveal the redox conditions of mantle melting from Archean to present. *Earth and Planetary Science Letters*, *288*(1-2), 255–267. https://doi.org/10.1016/j.epsl.2009.09.029

DePaolo, D. J. (2004). Calcium isotopic variations produced by biological, kinetic, radiogenic and nucleosynthetic processes. *Reviews in Mineralogy and Geochemistry*, *55*(1), 255–288. https://doi.org/10.2138/gsrmg.55.1.255

Embley, R. W., Chadwick, W., Perfit, M. R., & Baker, E. T. (1991). Geology of the northern Cleft Segment, Juan de Fuca Ridge: Recent lava flows, sea-floor spreading, and the formation of megaplumes. *Geology*, *19*, 771–775. https://doi.org/10.1130/0091-7613(1991)019

Embley, R. W., Murphy, K. M., & Fox, C. G. (1990). High-resolution studies of the summit of Axial volcano. *Journal of Geophysical Research*, *95*(B8), 12,785–12,812. https://doi.org/10.1029/JB095iB08p12785

Fantle, M. S., & DePaolo, D. J. (2005). Variations in the marine Ca cycle over the past 20 million years. *Earth and Planetary Science Letters*, *237*(1-2), 102–117. https://doi.org/10.1016/j.epsl.2005.06.024

Fantle, M. S., & Tipper, E. T. (2014). Calcium isotopes in the global biogeochemical Ca cycle: Implications for development of a Ca isotope proxy. *Earth-Science Reviews*, *129*, 148–177. https://doi.org/10.1016/j.earscirev.2013.10.004

Farkaš, J., Böhm, F., Wallmann, K., Blenkinsop, J., Eisenhauer, A., Van Geldern, R., et al. (2007). Calcium isotope record of Phanerozoic oceans: Implications for chemical evolution of seawater and its causative mechanisms. *Geochimica et Cosmochimica Acta*, *129*, 148–177. https://doi.org/10.1016/j.earscirev.2013.10.004

Farkaš, J., Buhl, D., Blenkinsop, J., & Veizer, J. (2007). Evolution of the oceanic calcium cycle during the late Mesozoic: Evidence from $\delta^{44/40}$Ca of marine skeletal carbonates. *Earth and Planetary Science Letters*, *253*(1-2), 96–111. https://doi.org/10.1016/j.epsl.2006.10.015

Feng, C., Qin, T., Huang, S., Wu, Z., & Huang, F. (2014). First-principles investigations of equilibrium calcium isotope fractionation between clinopyroxene and Ca-doped orthopyroxene. *Geochimica et Cosmochimica Acta*, *143*, 132–142. https://doi.org/10.1016/j.gca.2014.06.002

Feng, L.-P., Zhou, L., Yang, L., DePaolo, D. J., Tong, S.-Y., Liu, Y.-S., & Gao, S. (2017). Calcium isotopic compositions of sixteen USGS reference materials. *Geostands and Geoanalytical Research*, *41*(1), 93–106. https://doi.org/10.1111/ggr.12131

Fujii, T., & Scarfe, C. M. (1985). Composition of liquids coexisting with spinel lherzolite at 10 kbar and the genesis of MORBs. *Contributions to Mineralogy and Petrology*, *90*(1), 18–28. https://doi.org/10.1007/BF00373037

Green, D. H. (1973). Experimental melting studies on a model upper mantle composition at high pressure under water-saturated and water-undersaturated conditions. *Earth and Planetary Science Letters*, *19*(1), 37–53. https://doi.org/10.1016/0012-821X(73)90176-3

Griffith, E. M., Paytan, A., Caldeira, K., Bullen, T. D., & Thomas, E. (2008). A dynamic marine calcium cycle during the past 28 million years. *Science*, *322*(5908), 1671–1674. https://doi.org/10.1126/science.1163614

He, Y., Wang, Y., Zhu, C., Huang, S., & Li, S. (2017). Mass-independent and mass-dependent Ca isotopic compositions of thirteen geological reference materials measured by Thermal Ionisation Mass Spectrometry. *Geostands and Geoanalytical Research*, *41*(2), 283–302. https://doi.org/10.1111/ggr.12153

Heuser, A., & Eisenhauer, A. (2010). A pilot study on the use of natural calcium isotope ($^{44}Ca/^{40}Ca$) fractionation in urine as a proxy for the human body calcium balance. *Bone*, *46*(4), 889–896. https://doi.org/10.1016/j.bone.2009.11.037

Heuser, A., Eisenhauer, A., Gussone, N., Bock, B., Hansen, B. T., & Nägler, T. F. (2002). Measurement of calcium isotopes ($\delta^{44}Ca$) using a multicollector TIMS technique. *International Journal of Mass Spectrometry*, *220*(3), 385–397. https://doi.org/10.1016/S1387-3806(02)00838-2

Holmden, C., & Bélanger, N. (2010). Ca isotope cycling in a forested ecosystem. *Geochimica et Cosmochimica Acta*, *74*(3), 995–1,015. https://doi.org/10.1016/j.gca.2009.10.020

Huang, S., Farkaš, J., & Jacobsen, S. B. (2010). Calcium isotopic fractionation between clinopyroxene and orthopyroxene from mantle peridotites. *Earth and Planetary Science Letters*, *292*(3-4), 337–344. https://doi.org/10.1016/j.epsl.2010.01.042

Huang, S., Farkaš, J., & Jacobsen, S. B. (2011). Stable calcium isotopic compositions of Hawaiian shield lavas: Evidence for recycling of ancient marine carbonates into the mantle. *Geochimica et Cosmochimica Acta*, *75*(17), 4,987–4,997. https://doi.org/10.1016/j.gca.2011.06.010

Huang, S., & Jacobsen, S. B. (2017). Calcium isotopic compositions of chondrites. *Geochimica et Cosmochimica Acta*, *201*, 364–376. https://doi.org/10.1016/j.gca.2016.09.039

Jacobson, A. D., Andrews, M. G., Lehn, G. O., & Holmden, C. (2015). Silicate versus carbonate weathering in Iceland: New insights from Ca isotopes. *Earth and Planetary Science Letters*, *416*, 132–142. https://doi.org/10.1016/j.epsl.2015.01.030

Jaques, A., & Green, D. (1980). Anhydrous melting of peridotite at 0-15 Kb pressure and the genesis of tholeiitic basalts. *Contributions to Mineralogy and Petrology*, *73*(3), 287–310. https://doi.org/10.1007/BF00381447

John, T., Gussone, N., Podladchikov, Y. Y., Bebout, G. E., Dohmen, R., Halama, R., et al. (2012). Volcanic arcs fed by rapid pulsed fluid flow through subducting slabs. *Nature Geoscience*, *5*(7), 489–492. https://doi.org/10.1038/ngeo1482

Kamenetsky, V. S., Eggins, S. M., Crawford, A. J., Green, D. H., Gasparon, M., & Falloon, T. J. (1998). Calcic melt inclusions in primitive olivine at 43°N MAR: Evidence for melt-rock reaction/melting involving clinopyroxene-rich lithologies during MORB generation. *Earth and Planetary Science Letters*, *160*(1-2), 115–132. https://doi.org/10.1016/S0012-821X(98)00090-9

Kang, J.-T., Ionov, D. A., Liu, F., Zhang, C.-L., Golovin, A. V., Qin, L.-P., et al. (2017). Calcium isotopic fractionation in mantle peridotites by melting and metasomatism and Ca isotope composition of the Bulk Silicate Earth. *Earth and Planetary Science Letters*, *474*, 128–137. https://doi.org/10.1016/j.epsl.2017.05.035

Kang, J.-T., Zhu, H.-L., Liu, Y.-F., Liu, F., Wu, F., Hao, Y.-T., et al. (2016). Calcium isotopic composition of mantle xenoliths and minerals from eastern China. *Geochimica et Cosmochimica Acta*, *174*, 335–344. https://doi.org/10.1016/j.gca.2015.11.039

Klein, E. M., & Langmuir, C. H. (1987). Global correlations of ocean ridge basalt chemistry with axial depth and crustal thickness. *Journal of Geophysical Research*, *92*(B8), 8089–8115. https://doi.org/10.1029/JB092iB08p08089

Li, C.-F., Li, X.-H., Li, Q.-L., Guo, J.-H., Li, X.-H., & Yang, Y.-H. (2012). Rapid and precise determination of Sr and Nd isotopic ratios in geological samples from the same filament loading by thermal ionization mass spectrometry employing a single-step separation scheme. *Analytica Chimica Acta*, *727*, 54–60. https://doi.org/10.1016/j.aca.2012.03.040

Liu, F., Li, X., Wang, G., Liu, Y., Zhu, H., Kang, J., et al. (2017). Marine carbonate component in the mantle beneath the southeastern Tibetan Plateau: Evidence from magnesium and calcium isotope. *Journal of Geophysical Research: Solid Earth*, *122*, 9729–9744. https://doi.org/10.1002/2017JB014206

Liu, F., Zhu, H. L., Li, X., Wang, G. Q., & Zhang, Z. F. (2017). Calcium isotopic fractionation and compositions of geochemical reference materials. *Geostands and Geoanalytical Research*, *41*(4), 675–688. https://doi.org/10.1111/ggr.12172

Ma, J., Wei, G., Liu, Y., Ren, Z., Xu, Y., & Yang, Y. (2013). Precise measurement of stable neodymium isotopes of geological materials by using MC-ICP-MS. *Journal of Analytical Atomic Spectrometry*, *28*(12), 1926–1931. https://doi.org/10.1039/C3JA50229E

Magna, T., Gussone, N., & Mezger, K. (2015). The calcium isotope systematics of Mars. *Earth and Planetary Science Letters*, *430*, 86–94. https://doi.org/10.1016/j.epsl.2015.08.016

Nauret, F., Abouchami, W., Galer, S. J. G., Hofmann, A. W., Hémond, C., Chauvel, C., & Dyment, J. (2006). Correlated trace element-Pb isotope enrichments in Indian MORB along 18-20°S, Central Indian Ridge. *Earth and Planetary Science Letters*, *245*(1-2), 137–152. https://doi.org/10.1016/j.epsl.2006.03.015

Niu, Y. (1997). Mantle melting and melt extraction processes beneath ocean ridges: Evidence from abyssal peridotites. *Journal of Petrology*, *38*(8), 1047–1074. https://doi.org/10.1093/petroj/38.8.1047

Perfit, M. R., Fornari, D. J., Malahoff, A., & Embley, R. W. (1983). Geochemical studies of abyssal lavas recovered by DSRV ALVIN from the eastern Galapagos Rift-Inca Transform-Ecuador Rift: III. *Journal of Geophysical Research*, *88*(B12), 10,530–10,550. https://doi.org/10.1029/JB088iB12p10530

Price, R., Kennedy, A., Riggs-Sneeringer, M., & Frey, F. (1986). Geochemistry of basalts from the Indian Ocean triple junction: Implications for the generation and evolution of Indian Ocean ridge basalts. *Earth and Planetary Science Letters*, *78*(4), 379–396. https://doi.org/10.1016/0012-821X(86)90005-1

Raczek, I., Jochum, K. P., & Hofmann, A. F. (2003). Neodymium and strontium iosotope data for USGS reference materials BCR-1, BCR-2, BHVO-1, BHVO-2, AGV-1, AGV-2, GSP-1, GSP-2 and eight MPI-DING reference glasses. *Geostandards Newsletter*, *27*(2), 173–179. https://doi.org/10.1111/j.1751-908X.2003.tb00644.x

Rehkämper, M., & Hofmann, A. W. (1997). Recycled ocean crust and sediment in Indian Ocean MORB. *Earth and Planetary Science Letters*, *147*(1-4), 93–106. https://doi.org/10.1016/S0012-821X(97)00009-5

Rhodes, J. M., Morgan, C., & Liias, R. A. (1990). Geochemistry of Axial Seamount lavas: Magmatic relationship between the Cobb hotspot and the Juan de Fuca Ridge. *Journal of Geophysical Research*, *95*(B8), 12,713–12,733. https://doi.org/10.1029/JB095iB08p12713

Salters, V. J., & Stracke, A. (2004). Composition of the depleted mantle. *Geochemistry, Geophysics, Geosystems*, *5*, Q05004. https://doi.org/10.1029/2003GC000597

Simon, J. I., & DePaolo, D. J. (2010). Stable calcium isotopic composition of meteorites and rocky planets. *Earth and Planetary Science Letters*, *289*(3-4), 457–466. https://doi.org/10.1016/j.epsl.2009.11.035

Simon, J. I., DePaolo, D. J., & Moynier, F. (2009). Calcium isotope composition of meteorites, Earth, and Mars. *The Astrophysical Journal*, *702*(1), 707–715. https://doi.org/10.1088/0004-637X/702/1/707

Skulan, J., & DePaolo, D. J. (1999). Calcium isotope fractionation between soft and mineralized tissues as a monitor of calcium use in vertebrates. *Proceedings of the National Academy of Sciences of the United States of America*, *96*(24), 13,709–13,713. https://doi.org/10.1073/pnas.96.24.13709

Skulan, J., DePaolo, D. J., & Owens, T. L. (1997). Biological control of calcium isotopic abundances in the global calcium cycle. *Geochimica et Cosmochimica Acta*, *61*(12), 2505–2510. https://doi.org/10.1016/S0016-7037(97)00047-1

Smith, M. C., & Perfit, M. R. (1994). Petrology and geochemistry of basalts from the southern Juan de Fuca Ridge: Controls on the spatial and temporal evolution of Mid-Ocean Ridge Basalt. *Journal of Geophysical Research*, *99*(B3), 4787–4812. https://doi.org/10.1029/93JB02158.

Sobolev, A. V., Hofmann, A. W., Kuzmin, D. V., Yaxley, G. M., Arndt, N. T., Chung, S.-L., et al. (2007). The amount of recycled crust in sources of mantle-derived melts. *Science*, *316*(5823), 412–417. https://doi.org/10.1126/science.1138113

Sun, W., Bennett, V. C., Eggins, S. M., Arculus, R. J., & Perfit, M. R. (2003). Rhenium systematics in submarine MORB and back-arc basin glasses: Laser ablation ICP-MS results. *Chemical Geology*, *196*(1-4), 259–281. https://doi.org/10.1016/S0009-2541(02)00416-3

Sun, S.-S., & McDonough, W. F. (1989). Chemical and isotopic systematics of oceanic basalts: Implications for mantle composition and processes. *Geological Society, London, Special Publications*, *42*(1), 313–345. https://doi.org/10.1144/GSL.SP.1989.042.01.19

Teng, F.-Z., Li, W.-Y., Ke, S., Marty, B., Dauphas, N., Huang, S., et al. (2010). Magnesium isotopic composition of the Earth and chondrites. *Geochimica et Cosmochimica Acta*, *74*(14), 4150–4166. https://doi.org/10.1016/j.gca.2010.04.019

Urey, H. C. (1947). The thermodynamic properties of isotopic substances. *Journal of the Chemcal Society*, *562*, 562–581. https://doi.org/10.1039/jr9470000562

Valdes, M. C., Moreira, M., Foriel, J., & Moynier, F. (2014). The nature of Earth's building blocks as revealed by calcium isotopes. *Earth and Planetary Science Letters*, *394*, 135–145. https://doi.org/10.1016/j.epsl.2014.02.052

Verma, S. P. (1992). Seawater alteration effects on REE, K, Rb, Cs, Sr, U, Th, Pb and Sr-Nd-Pb isotope systematics of Mid-Ocean Ridge Basalt. *Geochemical Journal*, *26*(3), 159–177. https://doi.org/10.2343/geochemj.26.159

Weyer, S., & Ionov, D. A. (2007). Partial melting and melt percolation in the mantle: The message from Fe isotopes. *Earth and Planetary Science Letters*, *259*(1-2), 119–133. https://doi.org/10.1016/j.epsl.2007.04.033

Workman, R. K., & Hart, S. R. (2005). Major and trace element composition of the depleted MORB mantle (DMM). *Earth and Planetary Science Letters*, *231*(1-2), 53–72. https://doi.org/10.1016/j.epsl.2004.12.005

Zhang, Z.-F., Zhu, H.-L., Liu, Y.-F., Zhu, J.-M., Kang, J.-T., Tan, D., et al. (2013). A new approach on measuring calcium isotopic compositions using ^{42}Ca-^{43}Ca double spike on Triton-TIMS. Abstract V51A-2626 Presented at the 2013 AGU Fall Meeting, San Francisco, CA.

Zhao, X., Zhang, Z., Huang, S., Liu, Y., Li, X., & Zhang, H. (2017). Coupled extremely light Ca and Fe isotopes in peridotites. *Geochimica et Cosmochimica Acta*, *208*, 368–380. https://doi.org/10.1016/j.gca.2017.03.024

Zhu, H. L., Zhang, Z. F., Wang, G. Q., Liu, Y. F., Liu, F., Li, X., & Sun, W. D. (2016). Calcium isotopic fractionation during ion-exchange column chemistry and Thermal Ionisation Mass Spectrometry (TIMS) determination. *Geostands and Geoanalytical Research*, *40*(2), 185–194. https://doi.org/10.1111/j.1751-908X.2015.00360.x